Dielectronic recombination on and electron-impact excitation of heliumlike argon

R. Ali, C. P. Bhalla, C. L. Cocke, M. Schulz,* and M. Stockli
J. R. Macdonald Laboratory, Department of Physics, Kansas State University, Manhattan, Kansas 66506-2604
(Received 6 February 1991)

We have measured cross sections for $\Delta n=1$ dielectronic recombination (DR) on He-like argon and found good agreement with theoretical calculations based on the Hartree-Fock atomic model. Experimental absolute cross sections were obtained by using the electron-energy dependence of yields of He-like and Li-like argon ions from the Kansas State University electron-beam ion source to measure the ratio of the DR cross section on He-like argon to the electron-impact-ionization cross section of Li-like argon and normalizing to the latter. The K x-ray emission spectra due to $\Delta n=1,2$ DR and $n=1\rightarrow 2$ electron-impact excitation of He-like argon were also observed with a Si(Li) detector placed at 0° relative to the electron-beam direction. By normalizing to the theoretical KLL integrated DR differential cross section, we obtained differential and partial differential DR cross sections and differential electron-impact excitation cross sections. We found good agreement with Hartree-Fock calculations for DR and with distorted-wave calculations for electron-impact excitation.

I. INTRODUCTION

Dielectronic recombination (DR) is a process in which an incident free electron undergoes a radiationless capture by an ionic (atomic) target X^{q+}, resulting in the formation of a doubly excited ion (atom) $(X^{(q-1)+})^{**}$ followed by a stabilizing radiation to yield an ion (atom) in either its ground state $X^{(q+1)+}$ or a singly excited state $(X^{(q-1)+})^{*}$:

$$e^{-}+X^{q+}\rightarrow(X^{(q-1)+})^{**}\rightarrow X^{(q-1)+}+\gamma_{\mathrm{DR}} \quad (1a)$$

$$\rightarrow(X^{(q-1)+})^{*}+\gamma_{\mathrm{DR}}\ . \quad (1b)$$

The process is resonant in the incident electron energy and the change in the principal quantum number of the core electron is designated by Δn. The DR process has been the subject of discussion since the early 1940s [1], but it was not until the 1960's and 1970's that its importance in determining the charge-state equilibrium in hot plasmas was widely recognized [2–5]. The first experimental measurements of DR cross sections were reported in 1983 for $\Delta n=0$ [6–8]. Numerous subsequent measurements have now been performed. Some complications were encountered in comparison with theory due to the fact that the experimental cross sections were enhanced by the effect of the electric fields present in the apparatus on unresolved resonances lying near the series limit. It has been experimentally shown that this enhancement can be substantial [9]. Recent high-resolution experiments have made it easier to compare with theory for $\Delta n=0$ transitions [10–12]. For $\Delta n=1,2$ transitions the DR resonances are sufficiently well separated that individual groups containing a small number of resonances are easily isolated and electric-field effects are reduced. Briand *et al.* [13] reported on the observation of the KLL DR resonances on $Ar^{12+,13+,14+,15+}$ in an electron-beam ion source (EBIS) by detecting the emitted x rays. Knapp *et al.* [14] used the Lawrence Livermore National Laboratory (LLNL) electron-beam ion trap (EBIT) to detect the emitted x rays due to DR on and electron-impact excitation (EIE) of Ni^{26+} and obtained absolute cross sections for the KLL resonances by normalizing to the calculated cross section for radiative recombination off resonance. Though excellent agreement with theory was obtained, isotropic stabilizing radiation was assumed, an assumption which has recently been called into question [15]. The EBIT was also used to measure DR on heliumlike molybdenum and neonlike gold [16], where the effect of the angular distribution of polarized x rays was included in the calculations, and to study DR into Rydberg levels of lithiumlike titanium [17]. Recently, Kilgus *et al.* [18] reported on DR measurements on O^{7+} using the electron cooling device in the heavy-ion Test Storage Ring in Heidelberg, where reasonable agreement with theory was obtained.

In an earlier paper [19], we reported on $\Delta n=1$ DR cross-section measurements on He-like argon. In comparing with theory, good agreement was obtained for the KLL and KLM groups, while discrepancies were observed for the KLN and higher resonances. In this work we present improved measurements of $\Delta n=1$ DR cross sections that do not show these discrepancies as well as measurements of $\Delta n=1,2$ DR differential cross sections at $\theta_{\mathrm{lab}}=0°$.

In addition, we present measurements for $n=1\rightarrow 2$ electron-impact-excitation differential cross sections for heliumlike argon. Marrs *et al.* [20] reported the first measurements of EIE on highly charged ions, where the LLNL EBIT was used to observe the L x-ray emission spectra at $\theta_{\mathrm{lab}}=90°$ from EIE of Ne-like barium. Cross sections were obtained by normalizing to radiative recombination cross sections. Though differential cross-section calculations are needed for the comparison to be fruitful, the measured $4\pi d\sigma/d\Omega(90°)$ were in support of the theoretical total cross sections. Here, we compare our measurements to theoretical calculations that take into account the angular distribution of the emitted radiation.

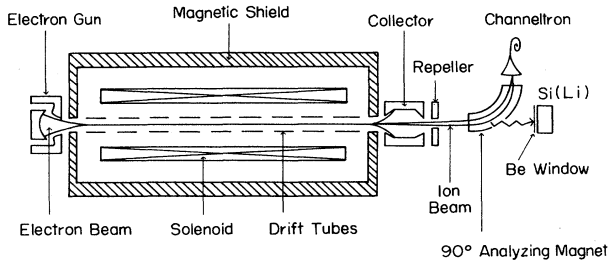

FIG. 1. Schematic of the EBIS and detection system.

II. EXPERIMENT AND RESULTS

Both the charge-state equilibrium and the x-ray experiments were performed using the Kansas State University EBIS, which has been described in detail elsewhere [21]. Figure 1 shows a schematic diagram of the experimental setup.

A. Charge-state equilibrium experiment

Under normal EBIS operation an electron beam (17 mA and energy between 2.1 and 3.8 keV in this experiment) is injected from the electron gun and compressed and confined by the magnetic field of the superconducting solenoid with a resulting current density of several hundred A/cm^2. The beam travels through the coaxial drift tubes and is absorbed by the axially symmetric collector at the exit of the solenoid. A small continuous flow of argon gas is injected into one drift tube. This injection region is nearly isolated from the cryogenic center region by the small conductance through and cryogenic pumping by the drift tubes. Electron-beam ionization of the injected argon results in the formation of low-charge ions that are then electrostatically injected into the 66-cm-long containment region in the center of the EBIS. In the containment region, successive electron-impact ionization drives the ions to higher charge states until the ionization potential exceeds the energy of the electron beam, at which point the charge state ceases to increase. For electron energies (E_e) less than 4.1 keV, the highest obtainable charge state is Ar^{16+}. The ions are trapped in the containment region radially by the space-charge potential of the electron beam and longitudinally by voltages applied to the drift tubes at the ends of the containment region. After some containment time (2.0 sec in this experiment was chosen to ensure achieving charge-state equilibrium and to optimize the Ar^{6+} fraction), the voltage of the containment region drift tubes is raised so that the ions are axially ejected from the source and emerge through the aperture in the collector, to be focused, analyzed in charge-to-mass ratio by a 90° magnet, and detected by a high-current channeltron. The charge-state distribution of argon ions was the same for containment times of 2.0, 3.0, and 4.0 sec, indicating charge-state equilibrium had been achieved, yielding about 96% Ar^{16+}, 4% Ar^{15+}, and less than 1% Ar^{14+} for an off-resonance E_e of 2.4 keV. The electron-beam energy is determined by the voltages applied to the electron gun and the containment region drift tubes plus a space-charge contribution caused by the electron beam itself. The electron-beam energy was varied by changing the voltage on the containment region drift tubes while keeping the electron-beam current fixed. Both the voltage on the containment region drift tubes and the analyzing magnet current was computer controlled. A full scan of the electron-beam energy range took about 30 min. The data from a large number of scans were averaged to minimize the effect of small fluctuations in source conditions. This experimental method has the advantage that there cannot be any metastables in the Ar^{16+} fraction.

The raw yields of $Ar^{14+,15+,16+}$ ions from the EBIS and their sum are shown as functions of the electron-beam energy in Fig. 2(a). The space-charge contributions to the electron-beam energy ($\Delta\Phi$) can be calculated accurately only if the radius and the current density profile of the electron beam are known. Instead, we chose to evaluate it from the observed location of the *KLL* resonance, whose energy is well known theoretically. On the *KLL* resonance $\Delta\Phi$ was 28 eV. Since the electron current remained fixed, this contribution was scaled with the inverse velocity of the electron according to

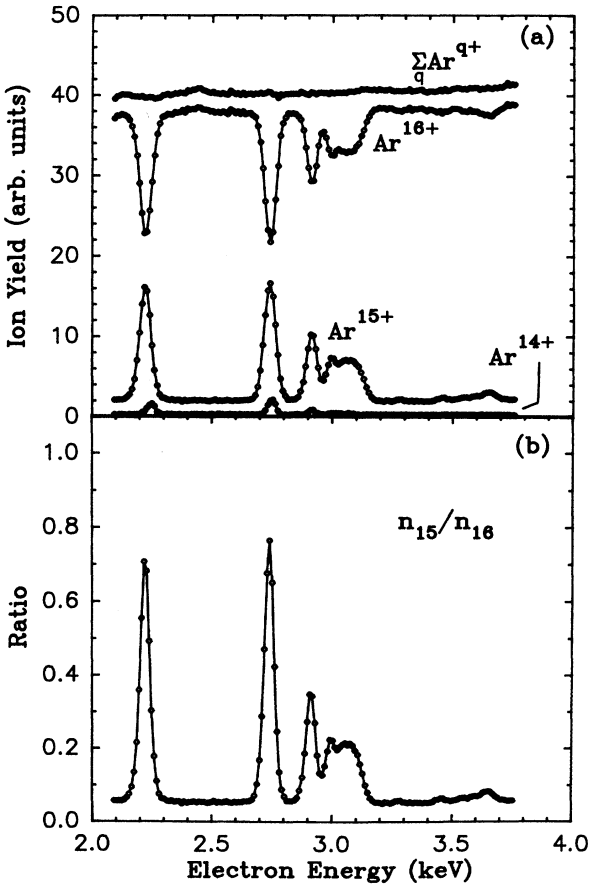

FIG. 2. Electron energy dependence of (a) the yields of Ar^{16+}, Ar^{15+}, Ar^{14+}, and their sum, and (b) the ratio n_{15}/n_{16}.

$$\Delta\Phi(E_e)=\Delta\Phi_{KLL}\sqrt{E_{eKLL}/E_e} \quad (2)$$

for other electron energies. The DR resonances onto the Ar^{16+} target are seen as depletions of the Ar^{16+} yield, and complimentary enhancements of the Ar^{15+} yield resulting from the radiative decay of the intermediate resonant states with configurations $1s2lnl'$, near energies of 2.22, 2.74, and 2.91 keV, corresponding to $n=2$ (KLL), 3 (KLM), and 4 (KLN), respectively. The KLn series limit ($n=\infty$), which is identical with the threshold for direct excitation, is seen at 3.14 keV. The figure also shows DR onto Ar^{15+}, as demonstrated by the enhancements of the Ar^{14+} yield, occurring at slightly higher energies than those onto Ar^{16+}. The fairly constant total argon-ion yield over the entire electron-beam energy range shows that the variation of E_e changes only the charge-state distribution of ions in the trap, not their total number.

The absolute DR cross sections were obtained from the following analysis. The number of Ar^{16+} ions is fed by electron-impact ionization on Ar^{15+}, and depleted by DR and radiative recombination (RR) on Ar^{16+} and capture collisions with residual gas in the EBIS. The rate equation for the population of Ar^{16+} is

$$\frac{dn_{16}}{dt}=(\sigma_i n_{15}-\sigma_{DR}n_{16}-\sigma_{RR}n_{16})\frac{j_e}{e}-\sigma_c n_{16}n_0\bar{v} , \quad (3)$$

where n_{15} and n_{16} are the numbers of Ar^{15+} and Ar^{16+} ions, j_e is the electron current density, e is the electron charge, $\bar{v}$ is the mean velocity of Ar^{16+} ions, n_0 is the density of the residual gas, σ_i is the ionization cross section of Ar^{15+}, and σ_{RR}, σ_{DR}, and σ_c are cross sections for the Ar^{16+} radiative recombination, dielectronic recombination, and capture on the residual gas, respectively. In equilibrium, $dn_{16}/dt=0$, and Eq. (3) gives

$$\sigma_{DR}=\sigma_i n_{15}/n_{16}-(\sigma_{RR}+\sigma_c n_0\bar{v}e/j_e) . \quad (4)$$

Since the second term on the right-hand side of Eq. (4) is slowly varying with E_e, σ_{DR} is simply given by $\sigma_i n_{15}/n_{16}$ minus a slowly varying background. Figure 2(b) shows the ratio n_{15}/n_{16} as a function of E_e. In Fig. 3 we show a plot of σ_{DR} deduced by subtracting a smooth background (obtained from a polynomial fit to nonresonant parts of the spectrum) from the experimental $\sigma_i n_{15}/n_{16}$, where σ_i was calculated from Ref. [22]. It should be noted that K excitation followed by ionization, which may appreciably enhance the ionization of Li-like ions above the K direct excitation threshold [23], does not affect σ_i used for E_e below 3.08 keV. Though similar equilibrium equations for other charge states would reveal couplings, for example, between n_{15} and n_{14}, the validity of Eq. (4) is not affected. DR onto Ar^{15+} serves only to deplete the population of both Ar^{15+} and Ar^{16+} but does not affect the n_{15}/n_{16} ratio. Furthermore, Eq. (4) does not depend on the identification of all processes that might deplete Ar^{16+}, such as electron-beam heating of the ions out of the trap. Any such process will be nonresonant in E_e, and will only give rise to an additional background term in Eq. (4).

For a certain DR resonance, $e^-+|i\rangle\rightarrow|s\rangle\rightarrow|f\rangle+\gamma_{DR}$, the resonant electron energy is $E_r=E_s-E_i$, where E_i and E_s are the energies of the initial state $|i\rangle$ and the resonant state $|s\rangle$. The resonance cross section has the typical Lorentzian shape and is given by

$$\sigma_{DR_r}(E_e)=\frac{\pi\hbar^2}{2m_eE_e}\frac{g_s}{2g_i}\frac{\Gamma_a(s\rightarrow i)\Gamma_r(s\rightarrow f)}{(E_e-E_r)^2+\Gamma_T^2(s)/4} . \quad (5)$$

In Eq. (5), g_s and g_i are the statistical weights of $|s\rangle$ and $|i\rangle$, $\Gamma_T(s)$ is the total width of $|s\rangle$, $\Gamma_a(s\rightarrow i)$ and $\Gamma_r(s\rightarrow f)$ are the contributions to $\Gamma_T(s)$ from the Auger

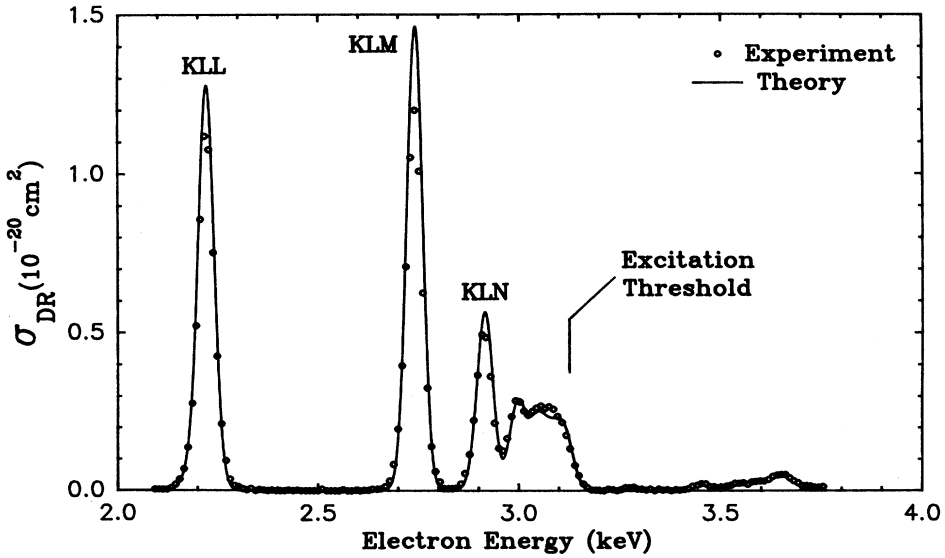

FIG. 3. Cross sections for dielectric recombination on heliumlike Ar. The points are the extracted cross sections as discussed in the text. The solid line is the theoretical calculation folded into the experimental resolution function.

transition $|s\rangle \rightarrow |i\rangle$ and the radiative transition $|s\rangle \rightarrow |f\rangle$. If the total width is much smaller than the width of the experimental energy resolution function, the Lorentzian factor approaches a δ function and Eq. (5) becomes

$$\sigma_{\mathrm{DR}_r}(E_e)=\frac{\pi^2\hbar^2}{2m_eE_e}\frac{g_s}{g_i}\frac{\Gamma_a(s\rightarrow i)\Gamma_r(s\rightarrow f)}{\Gamma_T(s)}\delta(E_e-E_r)\ . \tag{6}$$

When folded into the electron energy experimental resolution function $f(E_e)$, σ_{DR_r} becomes

$$\sigma_{\mathrm{DR}_r}(E_e)=\frac{\pi^2\hbar^2}{2m_eE_e}\frac{g_s}{g_i}\frac{\Gamma_a(s\rightarrow i)\Gamma_r(s\rightarrow f)}{\Gamma_T(s)}f(e_e)\ . \tag{7}$$

We take $f(E_e)$ to be a Gaussian given by

$$f(E_e)=\frac{1}{\sqrt{2\pi}\sigma}\exp\left[\frac{-(E_e-E_r)^2}{2\sigma^2}\right]\ . \tag{8}$$

The parameter σ measures the width of the experimental electron energy spread obtained here by fitting the theoretical curve for the *KLL* resonance to the experimental data. The value obtained was 18 eV corresponding to a full width at half maximum (FWHM) of 42 eV. Rewriting Eq. (7) in terms of the autoionization rate A_a, the radiative rate A_r, and the total rate A_T, we get

$$\sigma_{\mathrm{DR}_r}(E_e)=\frac{\pi^2\hbar^2}{2m_eE_e}F_2^*(s\rightarrow f)f(E_e)\ , \tag{9}$$

where the resonance strength is $F_2^*(s\rightarrow f)\equiv(g_s/g_i)[A_a(s)A_r(s\rightarrow f)/A_T(s)]$. The total theoretical DR cross section was obtained by summing the individual resonances,

$$\sigma_{\mathrm{DR}}(E_e)=\sum_r\sigma_{\mathrm{DR}_r}(E_e)\ . \tag{10}$$

The corresponding Auger energies (E_r) and all the rates for the doubly excited Li-like argon were calculated explicitly, using the Hartree-Fock atomic model [24], for the following cases: $1s2pnp$ ($n=2$–8), $1s2pns$ ($n=2$–8), $1s2pnd$ ($n=3$–6), $1s2pnf$ ($n=4,5$), and $1s2snp$ ($n=2$–8). The n^{-3} scaling law was used to obtain the resonance strengths for the above configurations but higher n, up to $n=20$. The scaled strengths are given by [25]

$$F_2^*(n)=\left[\frac{n_m}{n}\right]^3F_2^*(n_m)\ , \tag{11}$$

where n_m is the maximum n for which explicit calculations were done for each case mentioned above. The corresponding Auger energies for these high-n states were obtained from

$$E_n=3140-\frac{13.6Z^2}{n^2}\ , \tag{12}$$

where E_n is in units of eV, 3140 eV is the average direct excitation threshold ($1s^2\rightarrow 1s2l$) of Ar^{16+}, and $Z=16$.

TABLE I. Integrated experimental and theoretical DR cross sections (in 10^{-19} cm^2 eV) and their ratios.

Resonance	S_{expt}	S_{theor}	$S_{\mathrm{expt}}/S_{\mathrm{theor}}$
KLL	5.942	6.588	0.90
KLM	6.160	7.233	0.85
KLN[a]	2.663	2.857	0.93

[a]S calculated up to $E_e=2.96$ keV corresponding to the lowest point on the right-hand side of the *KLN* resonance.

The theoretical results so obtained are shown as a solid line in Fig. 3 and are in good agreement with experiment. To provide a comparison of theory and experiment that is independent of our choice of the width of the experimental resolution function, we present in Table I the experimental and theoretical integrated cross sections (S) and their ratios.

The discrepancies we had in our earlier results were traced to a channel-plate detector saturation effect. The signal strength, representing the ion yield, varies linearly with the instantaneous current in the detector for currents below a certain threshold, and nonlinearly for higher ones. The earlier discrepancies resulted from having the yield of Ar^{16+} lying in the nonlinear zone over the whole electron energy range, while the yield of Ar^{15+} was partially in this zone for the *KLL* and *KLM* resonances and in the linear zone for higher resonances. A similar saturation effect was found for the channeltron used here, but all data presented here were taken with sufficiently low voltages on the channeltron to ensure linearity.

For the purpose of the experiment, the relative detector efficiency for the different charge states must be known. For charge states between 12^+ and 16^+, the channeltron signal was measured to be approximately proportional to the incident charge, and this proportionality was used to assign relative efficiencies for 14^+–16^+ ions. The constant total ion yield in the sum curve of Fig. 2(a) confirms the validity of this efficiency assignment. Exclusive of any error in σ_i, we estimate an uncertainty of 9% on the experimental cross section due to background subtraction, reproducibility, and relative detector efficiency.

B. X-ray experiment

The purpose of this experiment was to further investigate DR on heliumlike argon by measuring differential and partial differential cross sections at $\theta_{\mathrm{lab}}=0°$ and to measure the electron-impact-excitation differential cross section of heliumlike argon at the same angle. Since DR processes onto Ar^{15+} occur at electron energies that overlap with those of DR onto Ar^{16+} and give rise to x rays with overlapping energies, it is important to have a pure Ar^{16+} target for such an experiment. In Fig. 4 we show the time evolution of the fraction of Ar^{16+} which was initially maximized by setting the electron-beam energy to a nonresonant value for 2 sec and switched onto the *KLL* resonance at $t=0$. By switching the electron en-

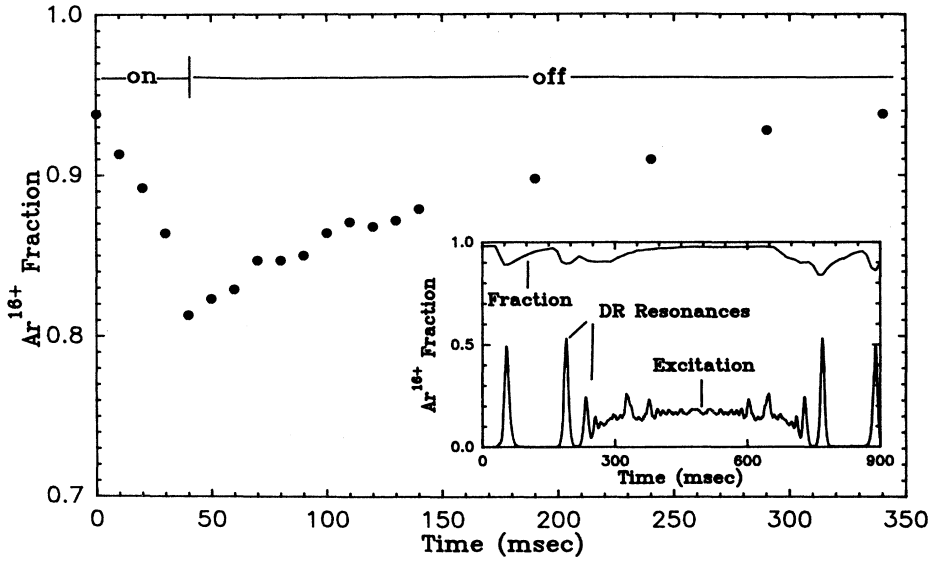

FIG. 4. Time evolution of the Ar^{16+} fraction for on- and off-resonance electron energies as discussed in the text. Inset: scanning time dependence of the Ar^{16+} fraction. A plot of the K x-ray yield is also shown in the inset to allow the association of each time with the corresponding electron energy.

ergy to a resonant value, the Ar^{16+} fraction dropped down by 13% in about 40 msec. A recovery time of 300 msec at a nonresonant E_e was then needed for the fraction to assume its initial value, demonstrating that the time constant for charge-state equilibrium on resonance is appreciably smaller than for off-resonance values. This short time constant on resonance energies required a modification to the experimental technique of part A in order to minimize the fraction of impurities.

The basic difference in the experimental technique from that of part A was that the argon-ion inventory was first prepared in the previously mentioned abundances by a 10-mA 2.4-keV electron beam for 2.0 sec before scanning the electron-beam energy. After 2.0 sec of cooking time, the electron-beam energy was scanned between 2.1 and 3.8 keV up and down ten times in 6.0 sec before the ions were ejected and a new cycle started. This guaranteed that the electron energy did not spend enough time on any resonance to strongly affect the charge-state equilibrium. The inset of Fig. 4 shows the scanning time dependence of the fraction of Ar^{16+} for an up-down scan of 900 msec. Depletions of the fraction are seen at such times where the electron energy is resonant and recovery is observed otherwise. The data shows that the margin of error due to the target impurity cannot exceed 15%. This error should be even smaller, since lost DR processes onto Ar^{16+} are partially substituted for by DR onto Ar^{15+}.

The x rays were detected during the scanning time as a function of the electron-beam energy by a Si(Li) detector placed at 0° relative to the electron-beam direction. The Si(Li) was 2.5 m from the EBIS center and viewed the EBIS interior through the collector aperture and a 25-μm Be window. The solid angle subtended by the detector was $4\pi\times10^{-6}$ sr.

Shown in Fig. 5 is a two-dimensional spectrum of the data collected in the event mode in this experiment. The horizontal and vertical axes represent the incident electron energy and the stabilizing x-ray energy, respectively. A physical process occurring at electron energy E_e and leading to x-ray production of energy E_x is represented by a dot whose coordinates are (E_e,E_x). The area of each dot reflects the number of counts in that channel. A number of isolated peaks are seen at various locations; these represent DR resonances. The continua extending from $E_e\approx2.95$ keV to the end are due to both DR and EIE.

By constructing two-dimensional windows, various parts of the spectrum could be projected onto the electron energy axis. A normalization factor was obtained by projecting the total two-dimensional spectrum onto the E_e axis and subtracting a smooth background and then normalizing the area under the experimental KLL resonance to the theoretical integrated KLL differential cross section.

The differential x-ray cross section for a transition $|s\rangle\rightarrow|f\rangle$ is given, when E_e is less than the $n=1\rightarrow n=2$ excitation threshold, by [26]

$$\frac{d\sigma_r(\theta_{\rm lab})}{d\Omega}=\frac{1}{4\pi}[1+\beta_r(J_i,J_s,J_f)P_2(\theta_{\rm lab})]\sigma_{\rm DR_r}(E_e)\ , \tag{13}$$

where β_r is the asymmetry parameter, J is the total angular momentum, and $P_2(\theta)$ is the Legendre polynomial of order 2. For the case discussed here

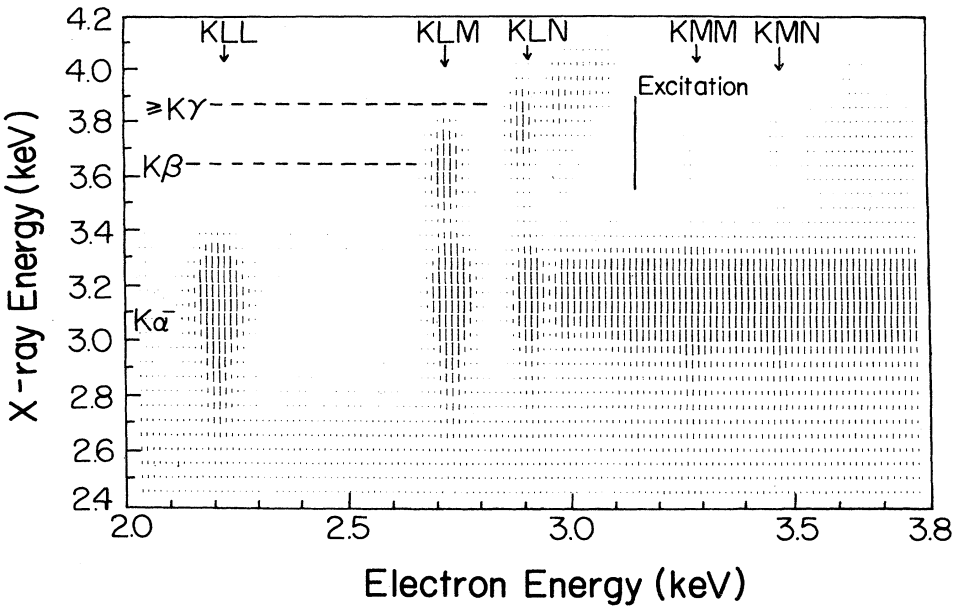

FIG. 5. A two-dimensional spectrum of Ar K x-ray energy vs electron energy. The peaks represent dielectric recombination resonances and the continua represent contributions from both dielectric recombination and electron-impact excitation.

$$\frac{d\sigma(\theta_{\rm lab}=0°)}{d\Omega}=\sum_r \frac{d\sigma_r(\theta_{\rm lab}=0°)}{d\Omega} . \tag{14}$$

In Fig. 6 we show the normalized experimental results as well as the theoretical calculations. As in part A, the theoretical calculations were folded into the experimental resolution function whose FWHM was 40 eV. Restricting ourselves first to $\Delta n=1$ DR, we show in Table II a comparison of the theoretical and normalized experimental integrated differential cross sections for the KLL, KLM, and KLN resonances. Projections of the parts of the two-dimensional spectrum corresponding to $K\alpha$, $K\beta$, $K\gamma$, and higher x rays, were also obtained, and, after background subtraction, were normalized and compared to the theory as presented in Fig. 7 and Table III. Tables II and III show good agreement between theory and ex-

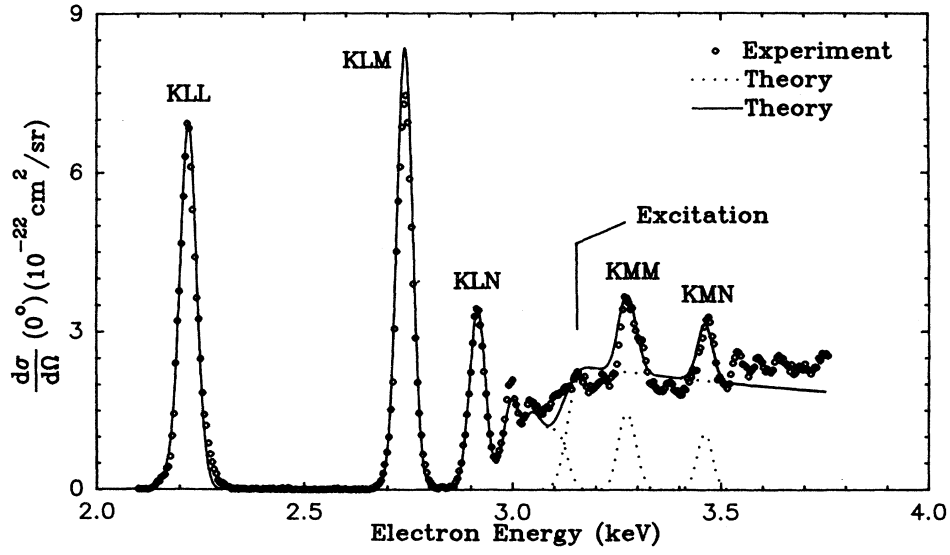

FIG. 6. Differential cross sections at $\theta_{\rm lab}=0°$ for K x-ray production due to dielectric recombination on and electron-impact excitation of Ar^{16+}. The points are the measured cross sections obtained through normalization as discussed in the text. The dotted lines are the individual contributions of dielectric recombination and electron-impact excitation folded into the experimental resolution function. The solid line is the sum of all contributions.

TABLE II. Integrated experimental and theoretical differential DR cross sections (in 10^{-20} cm^2 eV/sr) and their ratios.

Resonance	$\frac{dS_{\text{expt}}}{d\Omega}$	$\frac{dS_{\text{theor}}}{d\Omega}$	$\frac{dS_{\text{expt}}}{d\Omega} / \frac{dS_{\text{theor}}}{d\Omega}$
KLL	3.586	3.586	1.00
KLN	3.556	3.961	0.90
KLN[a]	1.639	1.652	0.99

[a]$dS/d\Omega$ calculated up to $E_e=2.96$ keV corresponding to the lowest point on the right-hand side of the *KLN* resonance.

TABLE III. $K\alpha$, $K\beta$, and $K\gamma$ contributions to the integrated experimental and theoretical differential DR cross sections (in 10^{-20} cm^2 eV/sr) and their ratios.

	Resonance	$\frac{dS_{\text{expt}}}{d\Omega}$	$\frac{dS_{\text{theor}}}{d\Omega}$	$\frac{dS_{\text{expt}}}{d\Omega} / \frac{dS_{\text{theor}}}{d\Omega}$
$K\alpha$	*KLL*	3.586	3.586	1.00
	KLM	2.930	3.266	0.90
	KLN[a]	1.241	1.199	1.04
$K\beta$	*KLM*	0.656	0.696	0.94
$K\gamma$	*KLN*[a]	0.418	0.446	0.94

[a]$dS/d\Omega$ calculated up to $E_e=2.96$ keV corresponding to the lowest point on the right-hand side of the *KLN* resonance.

periment where differences are within the estimated experimental error of 15%.

Figure 7 reveals many interesting features. A first observation is that the decay transitions are dominated by those giving rise to $K\alpha$ x rays, though $K\beta$ and $K\gamma$ transitions are also possible for the *KLM* and *KLN* resonances, for example. Another feature is the near absence of $K\beta$ transitions for the *KLN* resonance, which indicates that cascade transitions are quite weak. Although contributions from resonances higher than *KLN* to $K\gamma$ and higher K are observed, they need not necessarily be due to cascades but rather due to $K\delta$ and higher K transitions that we could not resolve from $K\gamma$. We also note that for the *KLM* resonance, the centroid of the $K\beta$ group is shifted by about 10 eV to the left of that of the $K\alpha$ group, indicating that Li-like doubly excited states giving rise to $K\beta$ x rays are in general populated at lower E_e than those giving rise to $K\alpha$. This shift is also predicted by the theory.

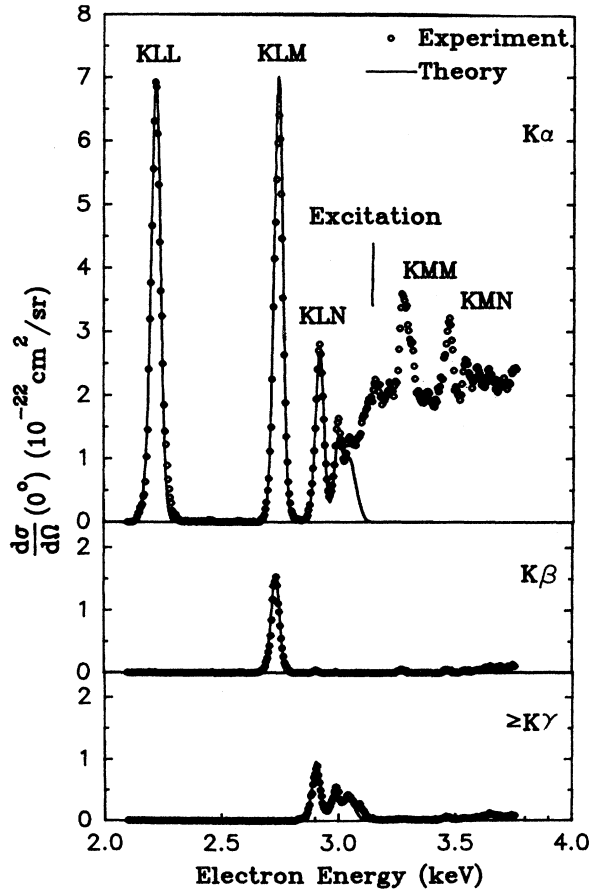

FIG. 7. Partial differential cross sections at $\theta_{\text{lab}}=0°$ for $\Delta n=1$ dielectronic recombination on Ar^{16+}. The points are the measured values and the solid lines are the theoretical calculations folded into the experimental resolution function.

$\Delta n=2$ DR results, both experimental and theoretical, are shown in Fig. 6 riding on the direct excitation continua. Theoretical rates were calculated in the same manner as for $\Delta n=1$ but for the states with configurations of the form $1s3l3l'$ and $1s3l4l'$. The dominant channel for the decay of these states is by Auger emission leading to $1s2l$ states, which decay radiatively to $1s^2\,{}^1S$. The differential x-ray cross sections were calculated for $\theta_{\text{lab}}=0°$. The experimental *KMM* and *KMN* areas were roughly estimated, and their ratios to theory were 0.98 and 0.93, respectively. An interesting feature observed is how pronounced the $\Delta n=2$ DR *KMM* and *KMN* resonances are compared to the charge-state experiment results. This occurs because these resonant states decay dominantly through *LMM* and *LMN* Auger decay followed by $K\alpha$ production, and thus do not achieve recombination.

Now we discuss the contribution of direct excitation, which leads to the continua. Zhang and Sampson [27] have performed a distorted-wave calculation of total and partial (different M_J) EIE cross sections (σ_{EIE}) at impact energies of 3.16, 3.2, 3.4, and 3.7 keV for the following cases: $1s^2\,{}^1S_0 \rightarrow 1s2s\,{}^3S_1, 1s2p\,{}^1P_1$, and $1s2p\,{}^3P_{0,1,2}$, whose thresholds are at impact energies of 3.107, 3.143, 3.125, 3.126, and 3.129 keV, respectively. Differential cross sections were obtained from these calculations using

$$\frac{d\sigma_{\text{EIE}}}{d\Omega}(E_e,\theta_{\text{lab}}) = W(\theta_{\text{lab}})\sigma_{\text{EIE}}(E_e)\ , \tag{15}$$

where the angular factors $W(\theta_{\text{lab}})$ were calculated at

$\theta_{lab}=0°$ for each of the above cases. A polynomial fit to the differential cross section was performed for each case and smooth curves were obtained from thresholds to $E_e=3.76$ keV which were then folded into the experimental resolution function and summed. The sum was added to the $\Delta n=1$ DR differential cross sections near the series limit, obtained by the n^{-3} scaling law, and to those of $\Delta n=2$. The possible contributions arising from the interference between the direct excitation and the DR resonances $1s3l3l'$ and $1s3l4l'$ have been neglected. It would not be possible to observe such contributions with the present resolution. As shown in Fig. 6, the experimental EIE differential cross sections agree well with those of Sampson and Zhang.

Electron-impact excitation near the threshold could be thought of as an extension of DR onto Ar^{16+}, but with the free electron going to the continuum rather than to a bound state. Hence, one would expect the x-ray production cross section due to DR resonances near the series limit to join smoothly with that of direct excitation at threshold. Surprisingly, a rapid rise in the cross section at threshold is observed in Fig. 6 and the $K\alpha$ part of Fig. 7. The explanation for this rise is that metastable ^3S and ^3P states populated by direct excitation have ample time to deexcite, due to the low collision rate inside the EBIS, thus giving $K\alpha$ x rays before engaging in other collisions. Thus these states must be, and have been, included in the EIE calculations. The corresponding DR resonances involve metastable cores coupled to Rydberg electrons, and are not included in the theoretical calculation. These resonances will contribute below threshold, but only for so high n that their Auger widths are comparable to their L-S electric-dipole-forbidden radiative widths. This probably occurs so close to threshold as to be virtually indistinguishable from the true threshold. This situation was investigated by Beiersdorfer *et al.* [17] for titanium.

III. CONCLUSION

Two experimental techniques were used to study dielectronic recombination on heliumlike argon. Experimental absolute cross sections obtained in the charge-state equilibrium experiment were in good agreement with theory. This agreement confirms that DR theory is on solid footing for Knn' transitions. The theory successfully predicted the details of the x-ray experiment as demonstrated by Tables II and III. We note that the experimental KLM resonance strength is consistently about ten percent below theory in both experiments. Electron-impact excitation cross sections obtained by normalizing DR were tested against distorted-wave calculations and good agreement was obtained. These results suggest the use of DR calculations as normalization to obtain other quantities of interest such as electron-impact ionization by studying the time evolution of charge states inside the EBIS.

ACKNOWLEDGMENTS

We thank H. L. Zhang and D. H. Sampson for communication of unpublished calculations of electron-impact-excitation cross sections. This work was supported by the Division of Chemical Sciences, Office of Basic Energy Sciences, Office of Energy Research, U. S. Department of Energy.

*Present address: Department of Physics, University of Missouri, Rolla, MO 65401.

[1] H. S. W. Massey, and D. R. Bates, Rep. Prog. Phys. **9**, 62 (1942).
[2] A. Burgess, Astrophys. J. **139**, 776 (1964).
[3] C. Jordan, Mon. Not. R. Astron. Soc. **142**, 499 (1969); **148**, 17 (1970).
[4] H. Summers, Mon. Not. R. Astron. Soc. **169**, 663 (1974).
[5] V. L. Jacobs, J. Davis, P. C. Kepple, and M. Blaha, Astrophys. J. **211**, 605 (1977); **215**, 106 (1977).
[6] J. B. A. Mitchell, C. T. Ng, J. L. Forand, D. P. Levac, R. E. Mitchell, A. Sen, D. B. Miko, and J. Wm. McGowan, Phys. Rev. Lett. **50**, 335 (1983).
[7] D. S. Belic, G. H. Dunn, T. J. Morgan, D. W. Mueller, and C. Timmer, Phys. Rev. Lett. **50**, 339 (1983).
[8] P. F. Dittner, S. Datz, S. D. Miller, C. D. Moak, P. H. Stelson, C. Bottcher, W. B. Dress, G. D. Aston, N. Nesdkovic, and C. M. Fou, Phys. Rev. Lett. **51**, 31 (1983).
[9] A. Mueller, D. S. Belic, B. D. DePaola, N. Djuric, G. H. Dunn, B. W. Mueller, and C. Timmer, Phys. Rev. Lett. **56**, 127 (1986).
[10] P. F. Ditner, S. Datz, R. Hippler, H. F. Krause, P. D. Miller, P. L. Pepmiller, C. M. Fou, Y. Hahn, and I. Nasser, Phys. Rev. A **38**, 2762 (1988).
[11] L. H. Andersen, P. Hvelplund, H. Knudsen, and P. Kvistgaard, Phys. Rev. Lett. **62**, 2656 (1989).
[12] L. H. Andersen, J. Bolko, and P. Kvistgaard, Phys. Rev. A **41**, 1293 (1990).
[13] J. P. Briand, P. Charles, J. Arianer, H. Laurent, C. Goldstein, J. Dubau, M. Loulergue, and F. Bely-Dubau, Phys. Rev. Lett. **52**, 617 (1984).
[14] D. A. Knapp, R. E. Marrs, M. A. Levine, C. L. Bennett, M. H. Chen, J. R. Henderson, M. B. Schneider, and J. H. Scofield, Phys. Rev. Lett. **62**, 2104 (1989).
[15] C. P. Bhalla, Phys. Rev. Lett. **64**, 1103 (1990).
[16] D. A. Knapp, in Proceedings of the Fifth International Conference on the Physics of Highly Charged Ions, Giessen, Germany, 1990 [Z. Phys. D (to be published)].
[17] P. Beiersdorfer *et al.*, in Proceedings of the Fifth International Conference on the Physics of Highly Charged Ions, Giessen, Germany, 1990 [Z. Phys. D (to be published)].
[18] G. Kilgus, J. Berger, P. Blatt, M. Grieser, D. Habs, B. Hochadel, E. Jaeschke, D. Krämer, R. Neumann, G. Neureither, W. Ott, D. Schwalm, M. Steck, R. Stokstad, E. Szmola, A. Wolf, R. Schuch, A. Müller, and M. Wagner, Phys. Rev. Lett. **64**, 737 (1990).
[19] R. Ali, C. P. Bhalla, C. L. Cocke, and M. Stockli, Phys. Rev. Lett. **64**, 633 (1990).
[20] R. E. Marrs, M. A. Levine, D. A. Knapp, and J. R. Henderson, Phys. Rev. Lett. **60**, 1715 (1988).

[21] M. Stockli, J. Arianer, C. L. Cocke, and P. Richard, Nucl. Instrum. Methods Phys. Res., Sect. B **40/41**, 1020 (1989); M. Stockli, C. L. Cocke, and P. Richard, in *International Symposium Electron Beam Ion Sources and Their Applications,* edited by A. Herschovitch, AIP Conf. Proc. No. 199, Particles and Fields Series No. 38 (AIP, New York, 1989), p. 115.

[22] S. Younger, J. Quant. Spectrosc. Radiat. Transfer **26**, 329 (1981).

[23] D. H. Crandall, R. A. Phaneuf, D. C. Gregory, A. M. Howald, D. W. Mueller, T. J. Morgan, and G. H. Dunn, Phys. Rev. A **34**, 1757 (1986).

[24] C. P. Bhalla and T. W. Tunnel, J. Quant. Spectrosc. Radiat. Transfer **32**, 141 (1984).

[25] K. R. Karim and C. P. Bhalla, Phys. Rev. A **43**, 615 (1991).

[26] C. P. Bhalla, K. R. Karim, and M. Wilson, Nucl. Instrum. Methods (to be published).

[27] H. L. Zhang and D. H. Sampson (private communication).